Enhanced Gravity Anomaly Separation Using a Wiener and Preferential Bandpass Butterworth Filtering for Structural Identification in Telomoyo Geothermal Area

Indra Arifianto[1,2], Jun Nishijima[1], Arif Darmawan[3]

[1] Department of Earth Resources Engineering, Faculty of Engineering, Kyushu University, Fukuoka 819-0395, Japan.

[2] Department of Geological Engineering, Faculty of Engineering, Universitas Gadjah Mada, Yogyakarta 55281, Indonesia.

[3] Geo Dipa Energy Ltd., Aldevco Octagon Building Lt.2, Jl. Warung Jati Barat Raya No. 75, Jakarta, Indonesia.

indra.arifianto@mail.ugm.ac.id

Keywords: *Anomaly Separation, Wavelength filtering, Wiener filter, Butterworth filter, Gravity data processing*.

ABSTRACT

Accurate anomaly separation in gravity data is crucial for geophysical investigations, particularly in resource exploration and subsurface analysis. Traditional wavelength filtering techniques often struggle to effectively balance noise suppression with anomaly preservation. In this study, we evaluate different wavelength filtering methods to identify the most effective approach for gravity anomaly separation. We propose a technique that combines the strengths of Wiener and Butterworth filters to achieve more accurate residual anomaly extraction than common high-pass and regular bandpass filtering. The Wiener filter is utilized for efficient noise reduction, i.e., mitigating terrain-induced effects, while the Butterworth filter is applied to isolate regional and residual anomalies. The methodology is first validated using synthetic gravity data generated from forward modeling of subsurface density variations, incorporating realistic terrain noise. Comparative analysis with common high-pass filtering techniques and regular bandpass filtering demonstrates the better performance of the proposed method in terms of accuracy and noise suppression. The approach is then applied to gravity data from the Telomoyo region, successfully extracting smoother residual anomalies with enhanced geological interpretability, especially in the subsurface structure delineation using edge detection analysis (e.g., Second Vertical Derivative and Improved Normalize Horizontal Tilt Angle). This method provides a robust and efficient tool for geophysical data processing, with significant implications for geothermal exploration, mineral prospecting, and subsurface structural analysis.

1. INTRODUCTION

Gravity data analysis is a critical component of geophysical exploration, playing a vital role in identifying subsurface density variations and delineating geological structures. A key challenge in gravity data interpretation is separating regional and residual anomalies, essential for understanding localized features such as faults, intrusions, or geothermal reservoirs. However, this separation is inherently complex, as various techniques including graphical residualization, surface fitting, empirical gridding, second vertical derivative (SVD), upward continuation, and wavelength filtering will produce divergent results (Telford et al. 1990). Further complicating the process is the presence of noise, particularly from terrain effects, which can obscure meaningful signals and compromise the accuracy of interpretations (Arifianto et al. 2024).

Conventional filtering methods, such as Bandpass, Butterworth, and Gaussian filters, implemented in widely used software like Oasis Montaj, have been extensively employed for anomaly separation. While these methods are effective in certain scenarios, they often struggle to adequately address noise contamination or achieve optimal separation of regional and residual components. To address these limitations, this study proposes a hybrid filtering approach that integrates the Wiener filter for noise reduction and the Butterworth bandpass filter for anomaly separation. The Wiener filter, renowned for its optimal noise suppression capabilities, is employed to mitigate terrain-induced noise (Gupta and Ramani 1980). In contrast, the Butterworth filter is utilized to isolate regional and residual anomalies based on their distinct frequency characteristics (Abdelfettah et al. 2014).

The proposed method is rigorously validated using synthetic gravity data generated through forward modeling of subsurface density variations. The results are systematically compared with those obtained from conventional filtering techniques in commercial software Oasis montaj, highlighting the superior performance of the hybrid approach. Subsequently, the method is applied to real gravity data from the Telomoyo region, where it successfully extracts the residual gravity anomaly, demonstrating its potential for geothermal exploration and subsurface characterization. By offering a robust and efficient tool for geophysical data processing, this study aims to enhance the accuracy and reliability of gravity data interpretation, ultimately contributing to improved exploration outcomes.

2. METHODOLOGY

2.1 Data Preparation

The primary dataset used in this study consists of synthetic gravity data generated through forward modeling, incorporating a terrain model to simulate realistic subsurface density variations (Nagy et al. 2000; Arifianto et al. 2024). The model includes deep regional and shallower local anomalies, with terrain effects introduced as noise to replicate real-world conditions (Figure 1). Terrain data from the Telomoyo region, along with real gravity data from previous studies in the same area (Arifianto et al. 2024), were utilized to ensure the model's relevance and accuracy.

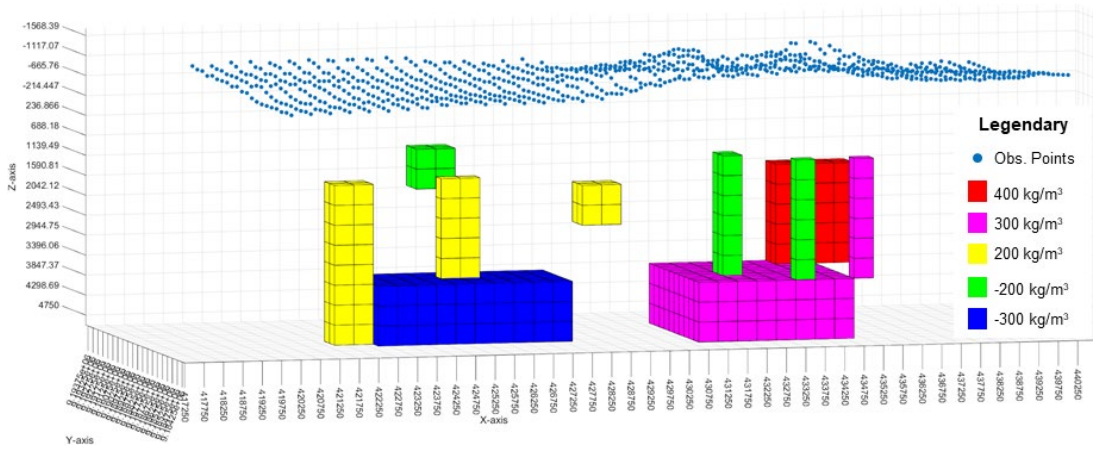

Figure 1. Subsurface synthetic density model under Telomoyo volcanic terrain

2.2 Gravity anomaly separation

The observed gravity anomaly ($G_{obs}(x,y)$) in general is composed of two primary components: a deep source, a long wavelength anomaly, and a shallow source ($G_d(x,y)$), short-wavelength anomaly ($G_s(x,y)$), as described by (Pawlowski 1994):

$$G_{obs}(x,y) = G_d(x,y) + G_s(x,y) \quad (1)$$

The power spectrum density function of the observed gravity anomaly (P_{obs}) is similarly expressed as the sum of the power spectra of the deep-source anomaly (P_d), the shallow source anomaly (P_s), and an error term E representing noise. This noise may arise from data acquisition inaccuracies, terrain effects, or imperfections in the spectral model (Guo et al. 2013).

$$P_{obs} = P_d + P_s + E \quad (2)$$

This method employs Fourier transformation combined with preferential filtering to separate the residual (short-wavelength) anomaly from the gravity data. The steps are as follows:

1. Fourier transform: The gravity anomaly ($G_{obs}(x,y)$) is transformed into the wavenumber domain $G_{obs}(k_x,k_y)$ using Fourier transform (Eq. 3). Padding is applied to the data to mitigate edge effects. The wavenumber grids are generated based on the dimensions and resolution of the gravity data and the magnitude of the wavenumber vector (k) is computed as Eq.4.

$$G_{obs}(k_x,k_y) = \mathcal{F}\{G_{obs}(x,y)\} \quad (3)$$

$$k = \sqrt{{k_x}^2 + {k_y}^2} \quad (4)$$

2. Power spectrum calculation: The power spectrum is calculated as the squared magnitude of the Fourier-transformed data. The radially averaged power spectrum $P_{obs}(k_x,k_y)$ is then computed and plotted as a natural logarithm against the wavenumber (k) (blue curve in Figure 2).

$$P_{obs}(k_x,k_y) = mean\left|G_{obs}(k_x,k_y)\right|^2 \quad (5)$$

3. Piece-wise linearization: The radially averaged logarithmic power spectrum is analyzed to determine the number of sections for piece-wise linearization and their respective wavenumber ranges (colored lines in Figure 2). Lower wavenumbers, corresponding to deeper layers, are divided into narrower sections, while higher wavenumbers, often dominated by noise, are segmented into broader ranges. Each section represents an equivalent source layer, with the source depth (h) estimated using the gradient of the fitted line (Spector and Grant 1970; Pawlowski 1994).

$$h = \frac{Slope_{\ fitted\ line}}{4\pi} \quad (6)$$

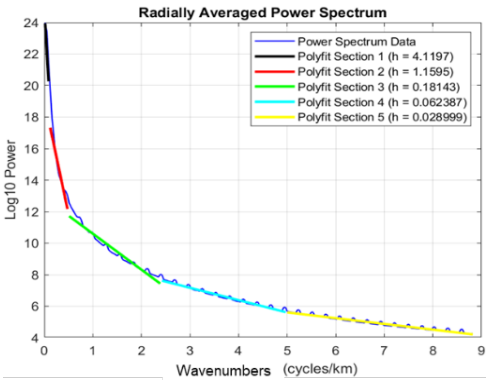

Figure 2. The plot of power spectrum versus wavenumber (blue line) and its fitting lines by using piece-wise linearization (color lines) with corresponding source depth anomaly (h).

4. Wiener filter for noise reduction: The Wiener filter ($H_{wiener}(k_x,k_y)$) is applied to suppress noise and enhance specific wavelength components associated with geological features (Gupta and Ramani 1980). The filter is designed by estimating the signal-to-noise ratio (SNR) from the power spectrum of the observed data (P_{noise})(Figure 3). The Wiener filter is then applied to the Fourier-transformed data ($G_{obs}(k_x,k_y)$) as follows:

$$H_{wiener}(k_x,k_y) = \frac{P_{obs}(k_x,k_y)}{P_{obs}(k_x,k_y) + P_{noise}} \quad (7)$$

$$G_{filtered}(k_x, k_y) = G_{obs}(k_x, k_y) \,.\, H_{wiener}(k_x, k_y) \qquad (8)$$

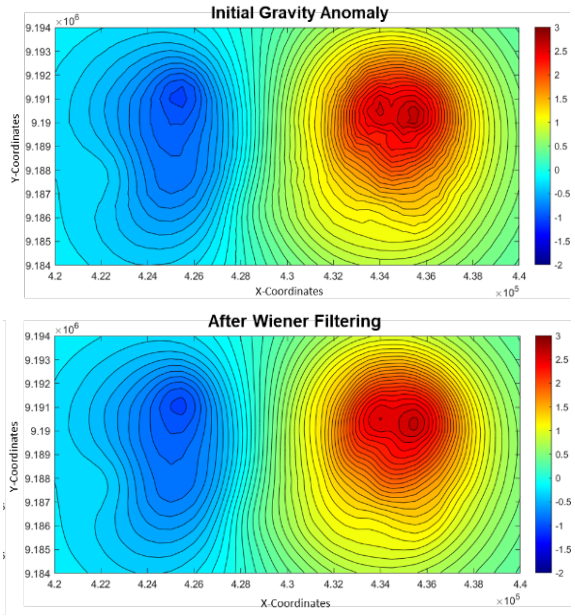

Figure 3. Gravity anomaly response of the subsurface synthetic model before and after the Wiener filter removes high-wavenumber noise due to acquisition noise and a small portion of terrain effects.

5. Butterworth bandpass filter for anomaly separation: The Butterworth bandpass filter ($H_{bwpass}(k_x, k_y)$) is constructed to isolate regional and residual components based on their frequency characteristics (Abdelfettah et al. 2014). The filter is designed with a specified order (n) to control the sharpness of the transition between the passband and stopband (Butterworth, 1930). For the regional component, a low-pass filter is applied with an upper cutoff wavenumber k_1 (Eq. 9). For the residual component, a high-pass filter is applied with k_1 and a low-pass filter with k_2 (Eq. 9). The filter responses are combined and normalized to the range [0, 1] for consistency (Figure 4).

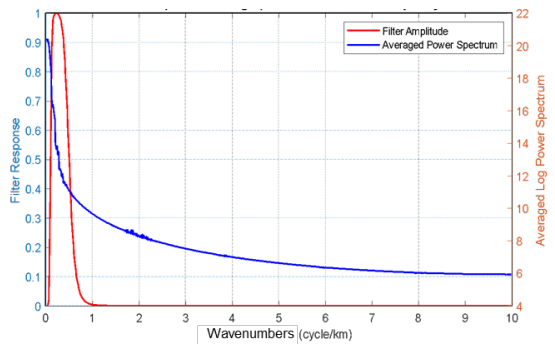

Figure 4. Plot of normalized filter response amplitude (red line) and average power spectrum (blue line) versus wavenumbers.

$$H_{bwpass}(k_x, k_y) = \begin{cases} \dfrac{1}{\left[1 + \left(\frac{k_{(x,y)}}{k_1}\right)^n\right]} & for\ k_{x,y} < k_1 \\ \dfrac{1}{\left[1 + \left(\frac{k_1}{k_{(x,y)}}\right)^n\right]} \cdot \dfrac{1}{\left[1 + \left(\frac{k_{(x,y)}}{k_2}\right)^n\right]} & for\ k_1 < k_{x,} \end{cases} \qquad (9)$$

6. Inverse Fourier Transform: Finally, the constructed filters are applied to the Fourier-transformed data, and the inverse Fourier transform is performed to obtain the separated regional and residual anomalies in the spatial domain ($G_{reg/residual}(x, y)$).

$$G_{reg/residual}(k_x, k_y) = G_{filtered}(k_x, k_y).H_{bwpass}(k_x, k_y) \qquad (10)$$

$$G_{reg/residual}(x, y) = \mathcal{F}^{-1}\{G_{obs}(k_x, k_y)\} \qquad (11)$$

3. RESULT AND DISCUSSION

3.1 Synthetic Forward Model

The synthetic test model consists of ten rectangular prisms with varying sizes, depths, and densities (Table 1). The larger prisms, R1 and R2, are positioned in deeper layers and are classified as regional anomalies (Figure 1). These anomalies could represent geological features such as laccoliths or lopoliths in volcanic regions, or sedimentary infill in a sedimentary basin. In contrast, the smaller prisms (L1–L8) are located at different depths and have varying dimensions, representing local anomalies. These features may correspond to geological structures such as sills or dikes in volcanic settings, or salt/mud diapirs in sedimentary basins.

Table 1. Synthetic subsurface body's location with corresponding density anomaly.

No	Anomaly Body	Depth (m) Bellow MSL	X-coord (m) UTM49S	Y-coord (m) UTM49S	Density anomaly (kg/m^3)
1	R1	3500 – 5000	423000 – 428000	9187000 – 9190000	- 300
2	R2	3500 – 5000	431000 – 435000	9186000 – 9191000	300
3	L1	1000 – 5000	422000 – 423000	9187500 – 9188500	200
4	L2	1000 – 2000	428000 – 429000	9186000 – 9187000	200
5	L3	500 – 3500	432000 – 432500	9187500 – 9188500	- 200
6	L4	1000 – 3500	425000 – 426000	9188500 – 9189000	200
7	L5	500 – 3500	433500 – 434000	9186000 – 9186500	- 200
8	L6	500 – 1500	425000 – 426000	9191000 – 9192000	- 200
9	L7	500 – 3500	435000 – 435500	9186000 – 9186500	300
10	L8	1000 – 3500	434000 – 436000	9190000 – 9191000	400

Furthermore, to simulate realistic conditions, the synthetic model incorporate variations in observation point elevations to account for terrain effects, which is act as noise in our data (Figure 5). The regional anomalies exhibit gravity variations ranging from -1.5 mGal to 2 mGal, whereas local anomalies range from -0.2 mGal to 1.8 mGal. The terrain-induced noise has an anomaly range of -0.8 mGal to 0.1 mGal. As a result, the total observed gravity anomaly in the synthetic model spans from -1 mGal to 2.5 mGal (Figure 5).

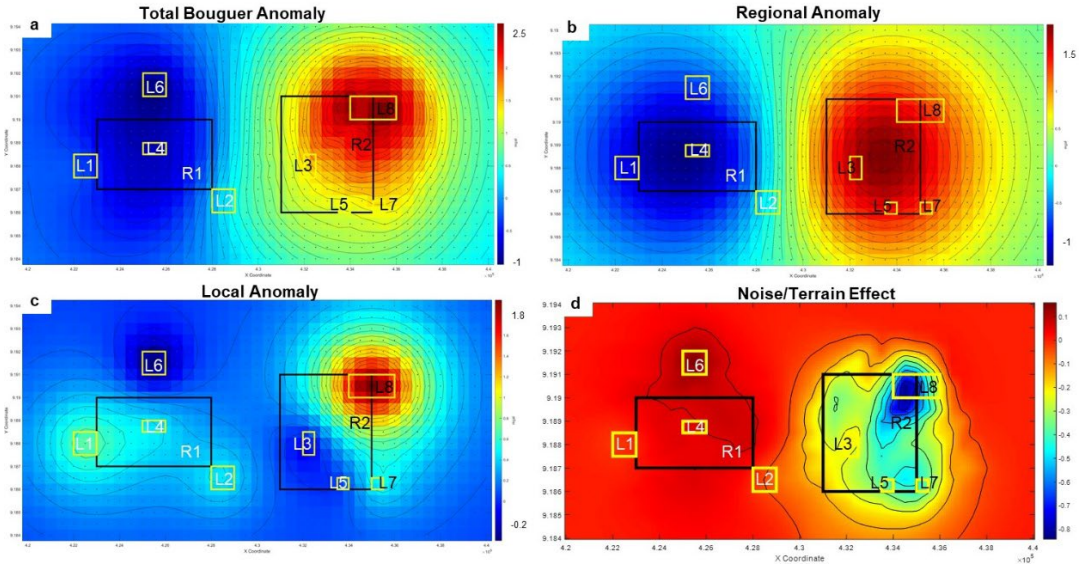

Figure 5. (a) Gravity anomaly from the synthetic model is also considered a complete Bouguer anomaly. (b) Regional anomaly gravity that is coming from deep and large source anomaly bodies. (c) Local gravity anomalies come from shallower depth and smaller dimension bodies and are considered residual anomalies. (d) Terrain effects are due to the different heights of observation points on the surface that follow the terrain and are considered as noise.

3.2 Comparison of The Filter Design in Synthetic Data

A radially averaged power spectrum analysis was performed using Oasis Montaj to guide wavelength filtering. The radially averaged power spectrum and depth estimation help distinguish between long-wavelength (low wavenumber) and short-wavelength (high wavenumber) components. Based on the gravity anomaly data, regional anomalies correspond to wavenumbers less than 0.165, which equal to a wavelength of approximately 6000 meters and a source depth of about 3.5 km (Figure 6). In contrast, local anomalies fall within a wavenumber range of 0.165 to 0.54, corresponding to wavelengths between 6000 and 1850 meters, with estimated source depths ranging from 3.5 km to 1.1 km (Figure 6).

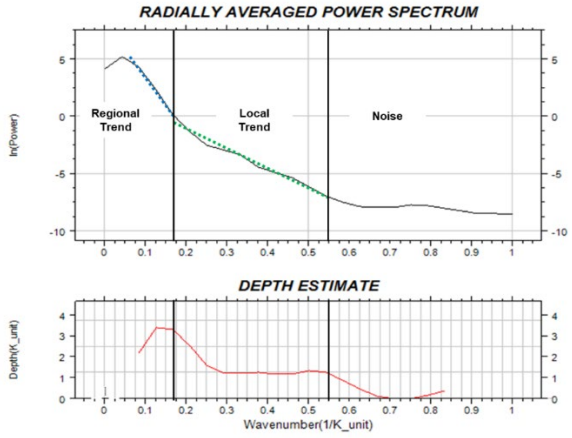

Figure 6. Radially averaged power spectrum from commercial software separates regional and local trends and corresponding depth estimation.

Regional and local anomalies are separated using our hybrid filtering method alongside standard filter designs available in commercial Oasis Montaj software, such as Gaussian high-pass, Butterworth high-pass, and regular bandpass filters. The wavelength filtering parameters e.g., regional wavenumber (regional trend) and residual wavenumber (regional trend), are determined based on the radially averaged power spectrum plot (in Figure 6) with some wavelength adjustments to optimize the filter response. The result of each filter response setting is presented as follows:

- The Gaussian high-pass filter is a smoothing filter that retains high wavenumbers (short wavelengths) to extract residual anomalies. This filter is based on an exponential function and gradually attenuates longer wavelengths. In this study, the Gaussian filter is applied with a cutoff wavelength of 7600 meters, and its corresponding filter response is shown in Figure 7a.

- The Butterworth high-pass filter follows the same equation as in Eq. 9 but applies a high-pass condition for wavenumbers $k_{x,y} > k_1$. The cutoff wavelength is also set at 7600 meters. A key advantage of the Butterworth filter over the Gaussian filter is its adjustable roll-off rate, controlled by the filter order (n). In this case, we use filter order n = 4, resulting in a smoother transition and more controlled attenuation (Figure 7b).

- The regular bandpass filter is designed to isolate a specific range of wavenumbers by passing or rejecting selected components from the data. However, the simple cutoff nature of this filter can introduce the Gibbs phenomenon, leading to ringing artifacts. This study applies the bandpass filter with a wavelength range of 7600 to 2700 meters (Figure 7c).

- Butterworth bandpass filter is employed to get a smoother residual anomaly and mitigate the ringing effect caused by the Gibbs phenomenon. By setting the filter order n = 4, we achieve a more gradual transition while preserving essential anomaly characteristics. The

ISSN 2703-4275

selected bandpass wavelength range for residual anomaly extraction is 7600 meters to 2700 meters, corresponding to a wavenumber range of 0.13 to 0.37 (Figure 7d).

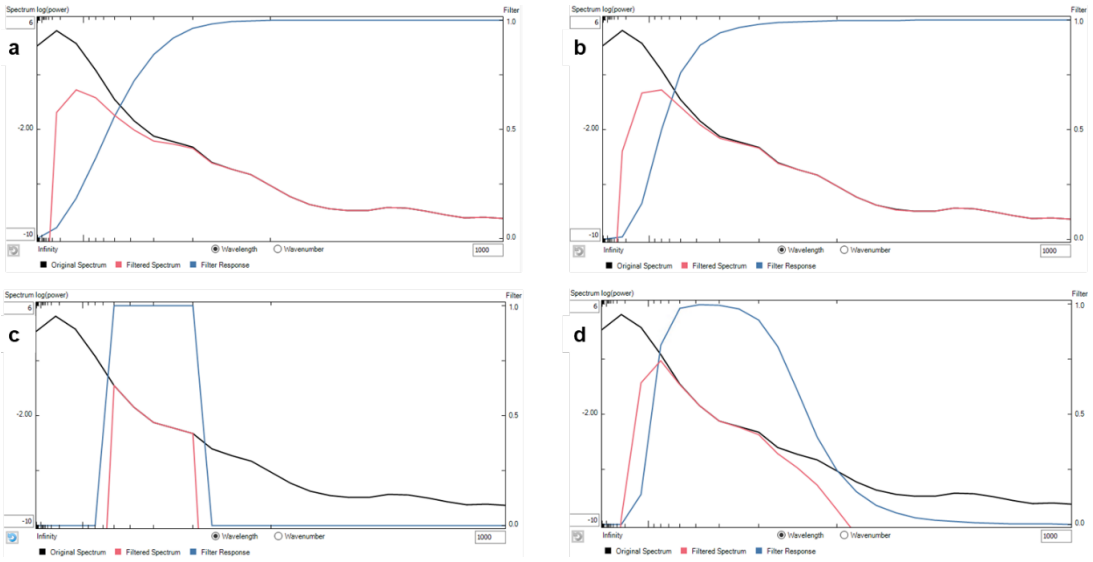

Figure 7. Filter design and its corresponding filtered spectrum using different filter techniques: (a) Gaussian high-pass, (b) Butterworth high-pass, (c) Regular band-pass, and (d) Butterworth band-pass.

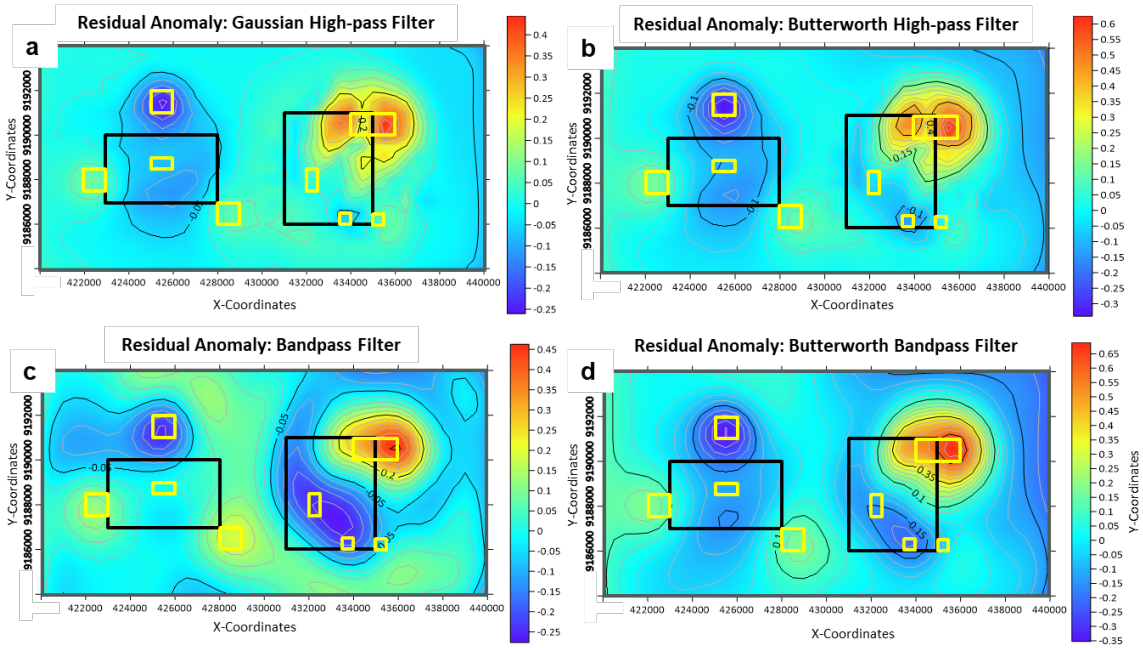

Figure 8. The residual anomaly results from a) Gaussian high-pass filter, b) Butterworth high-pass filter, c) Regular bandpass filter, and d) Butterworth bandpass filter.

The residual anomaly results from both Gaussian and Butterworth high-pass filter indicate that terrain effects are still present, as all short-wavelength components are retained in the filtered data (Figures 8a & 8b). This highlights a limitation of high-pass filtering in fully isolating residual anomalies from terrain-induced noise. The Gaussian filter produces a lower amplitude response than the Butterworth filter due to its fixed, smooth attenuation curve. In contrast, the Butterworth filter allows for adjustable filter order (n), enabling control over the transition between pass and stop bands, which can be tuned for either a gradual or steeper cutoff.

In the bandpass filtering approach, both the regular and Butterworth bandpass filters produce a smoother residual anomaly, significantly reducing terrain-related noise (Figure 8c & 8d). However, a key drawback of bandpass filtering is its susceptibility to ringing artifacts in the residual anomaly map due to the Gibbs phenomenon, particularly at higher wavenumbers. Despite this, the Butterworth filter tends to yield a higher amplitude response, attributed to its smoother filter transition, which helps preserve critical anomaly features.

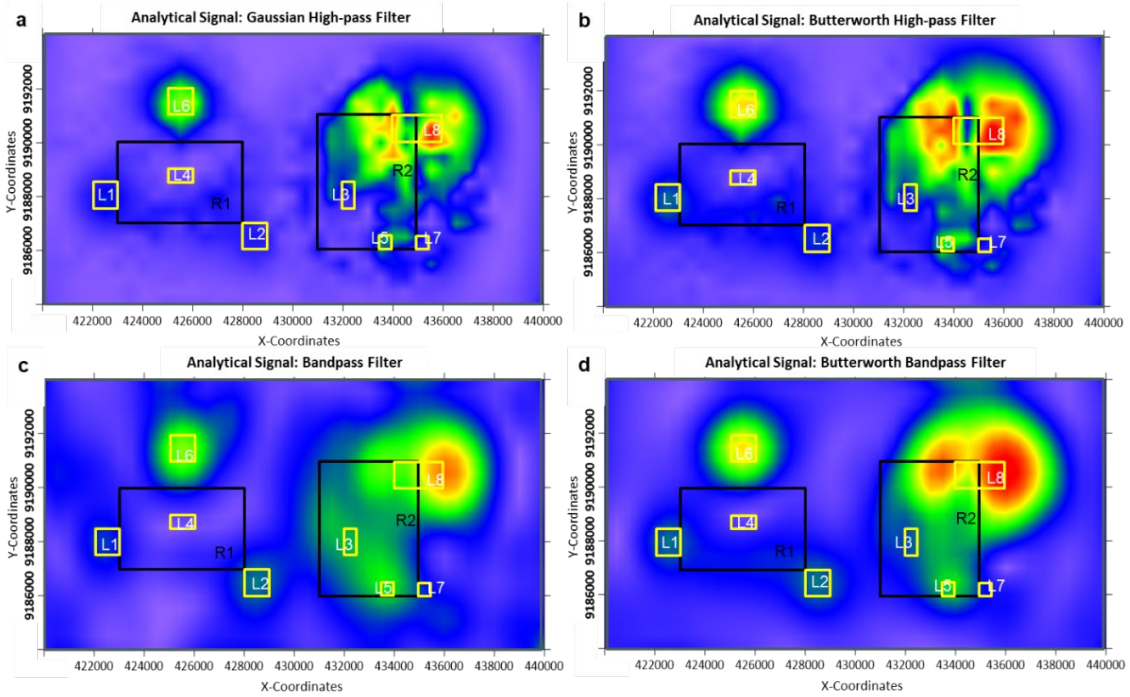

Figure 9. Analytical signal of the residual anomaly from different filtering types: a) Gaussian high-pass filter, b) Butterworth high-pass filter, c) regular bandpass filter, and d) Butterworth bandpass filter.

The analytical signal was applied to further evaluate the effectiveness of different filtering techniques, which enhances source boundaries by utilizing the squared sum of derivatives in the *x*, *y*, and *z* directions (Saibi et al. 2006). This method helps delineate subsurface structures more precisely. The analytical signal results reveal that the high-pass filter produces a scattered pattern near the R2 area, likely due to the effects of volcanic terrain. Additionally, the local anomaly L8 appears artificially divided into two separate bodies, which does not accurately reflect the true subsurface structure (Figures 9a & 9b).

In contrast, the bandpass filter improves anomaly delineation, particularly for the R2 anomaly, which exhibits a strong analytical signal response. However, in the Butterworth bandpass filter, the R2 anomaly is still detected but with a weaker signal, suggesting that it is less influenced by residual filtering effects (Figures 9c & 9d). A key limitation of the bandpass filtering approach is that the L3 and L4 anomalies are relatively undetected. This is likely due to the gravity signal reversal caused by the regional anomaly, combined with the small size of L3 and L4, making their gravity response insignificant compared to the broader regional signal.

Given the significant impact of terrain effects on local anomalies, which cannot be fully eliminated during standard gravity corrections, suppressing terrain effects remains the most practical approach. While it is theoretically impossible to perfectly separate regional and local anomalies due to their inherent density integration, the Butterworth bandpass filter proves to be the most effective at minimizing terrain-related noise compared to other filtering methods.

3.3 Hybrid Filter for Residual Anomaly Separation of Gravity Data Telomoyo Area

The first step in anomaly separation is analyzing the radially averaged power spectrum to estimate the wavelengths or wavenumbers corresponding to regional and local trends. The regional source depth is approximately 3.7 km, with wavelengths exceeding 5400 meters (equivalent to a wavenumber of less than 0.185). Meanwhile, the local source depth ranges from 0.6 km to 3.7 km, with wavelengths between 5400 meters and 1500 meters (equivalent to a wavenumber range of 0.185 to 0.7) (Figure 10). The regional source is interpreted as igneous rock intrusions, while the local sources are likely volcanic lava flows, sills, or dikes.

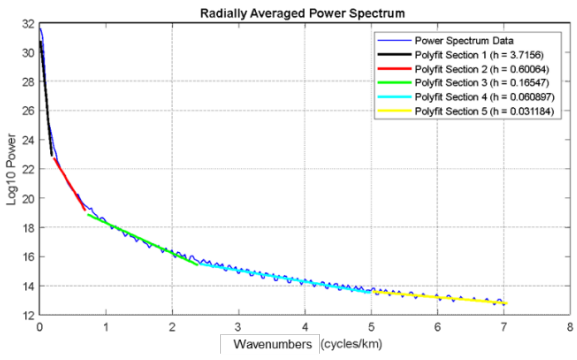

Figure 10. Power spectrum depth analysis in Telomoyo shows that the local anomaly depth source is from 0.6 km to around 3.7 km with wavelengths of 5400 meters to 1500 meters.

The residual gravity anomaly in the Telomoyo area ranges from 6 to -4 mGal. A positive anomaly is observed in the central valley between mountainous terrains, whereas

negative anomalies are mainly at mountain peaks (Figure 11a). Some of these anomalies may result from terrain effects, as Arifianto et al. (2024) suggested. However, certain anomalies could also be influenced by lower-density volcanic rocks, which integrate with the gravitational effects of topography.

To enhance interpretation, we apply Second Vertical Derivative (SVD), Analytical Signal (AS), and Improved Normalized Horizontal Tilt Angle (INH) for subsurface analysis.

- Second Vertical Derivative (SVD)
  SVD amplifies short-wavelength, high-frequency anomalies, effectively identifying shallow structures, density contrasts, and fault zones (Telford et al., 1990; Sumintadireja et al. 2018). In gravity surveys, SVD highlights density variations associated with faults, intrusions, and sedimentary basins (Sarkowi et al., 2021). However, SVD also amplifies random noise, particularly in areas with complex terrain. Wiener and Butterworth bandpass filtering are applied to mitigate this, resulting in a smoother anomaly map with clearer edge detection. The SVD results for the Telomoyo gravity data reveal similar trends to the residual anomaly map but with enhanced anomaly localization and reduced noise (Figure 11b). In this study, positive and negative anomalies are interpreted as igneous intrusions or could be shallow extrusive lava, exhibiting higher and lower densities, respectively, compared to the background density used in Bouguer and terrain corrections.

- Analytical Signal (AS)
  The analytical signal helps locate the subsurface anomaly locations, as anomaly bodies are detected directly above their causative sources (Saibi et al., 2006). In this study, bodies with AS values exceeding 0.1 mGal/m are interpreted as igneous intrusions, sills, dikes, or buried lava flows of the volcanic sequence in the Telomoyo area (Figure 11c).

- Improved Normalized Horizontal Tilt Angle (INH):
  The INH filter is used to delineate fault structures while minimizing the impact of noise (Li et al. 2014). Compared to the standard tilt angle method, INH provides better results in complex terrain because its normalization process reduces noise in low-gradient areas. The geological structures are identified by radian values around 1, aligning with previously mapped structural lineaments from Abdilah et al. (2024), with additional newly interpreted faults (Figure 11d).

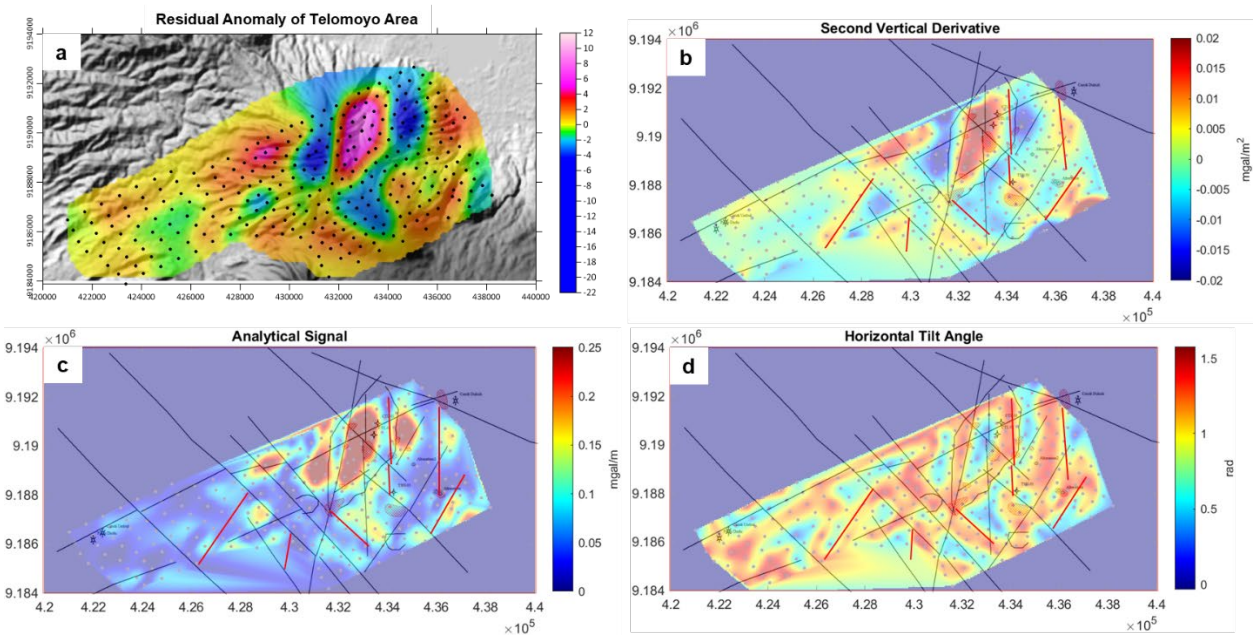

Figure 11. The residual anomaly from Wiener and Butterworth wavelength filtering (a) was then analyzed using edge detection Second Vertical Derivative (b), Analytical Signal (c), and Improved Normalized Horizontal Tilt Angle (d). The fault interpretation from Abdillah et al. (2024) is in black lines, with this study additional fault interpretation in red lines.

4. CONCLUSIONS

This study demonstrates that the hybrid Wiener–Butterworth filtering technique offers a robust and effective approach for gravity anomaly separation by combining the noise-suppression capability of the Wiener filter with the frequency-selective precision of the Butterworth bandpass filter. Synthetic data tests, incorporating realistic subsurface density variations and terrain-induced noise, confirmed the method's ability to accurately isolate both regional and residual anomalies. The Wiener filter effectively attenuates high-wavenumber noise, while the subsequent Butterworth filter, with its adjustable roll-off characteristics, enables a smoother transition between passband and stopband frequencies. This dual-step approach significantly reduces spectral artifacts such as the Gibbs phenomenon and ringing effects, which commonly degrade the resolution and interpretability of the anomaly maps.

When applied to real gravity data from the Telomoyo region, the hybrid filter further demonstrated its practical utility. Radially averaged power spectrum analysis provided a clear demarcation between long-wavelength regional and short-wavelength residual components. In combination with edge-detection techniques such as the Second Vertical Derivative (SVD), Analytical Signal (AS), and Improved Normalized Horizontal Tilt Angle (INH), the filtered results enhanced the delineation of subsurface structures. This improved clarity is critical for accurate geological interpretation in complex terrains. Overall, the hybrid Wiener–Butterworth filtering method represents a more accurate and reliable tool for gravity data processing, with strong potential for applications in geothermal exploration, volcanic studies, mineral prospecting, and structural geology.

ACKNOWLEDGEMENTS

This research was supported by the Japan International Cooperation Agency (JICA) through the provision of a scholarship and research funding, for which I am deeply grateful. I would also like to thank PT Geo Dipa Energy (Persero) Indonesia for the permission to use their data in this research. Lastly, I would like to extend my sincere thanks to my colleagues in the Geothermic Laboratory at the Department of Earth Resource Engineering, Kyushu University, for their invaluable discussions and input throughout the course of this research.

REFERENCES

Abdelfettah Y, Schill E, Kuhn P (2014) Characterization of geothermally relevant structures at the top of crystalline basement in Switzerland by filters and gravity forward modelling. Geophysical Journal International 199(1):226–241. https://doi.org/10.1093/gji/ggu255

Arifianto I, Nishijima J, Darmawan A (2024) Terrain Effects on Gravity and Magnetic Responses: Insights from Forward Modeling in Telomoyo Geothermal Exploration Area. In: Proceeding of International Symposium on Earth Science and Technology 2024. CINEST, Fukuoka, pp 496–501

Guo L, Meng X, Chen Z, Li S, Zheng Y (2013) Preferential filtering for gravity anomaly separation. Computers & Geosciences 51:247–254. https://doi.org/10.1016/j.cageo.2012.09.012

Gupta VK, Ramani N (1980) Some aspects of regional-residual separation of gravity anomalies in a Precambrian terrain. GEOPHYSICS 45(9):1412–1426. https://doi.org/10.1190/1.1441130

Li L, Huang D, Han L, Ma G (2014) Optimised edge detection filters in the interpretation of potential field data. Exploration Geophysics 45(3):171–176. https://doi.org/10.1071/EG13059

Nagy D, Papp G, Benedek J (2000) The gravitational potential and its derivatives for the prism. Journal of Geodesy 74(7–8):552–560. https://doi.org/10.1007/s001900000116

Pawlowski RS (1994) Green's equivalent-layer concept in gravity band-pass filter design. GEOPHYSICS 59(1):69–76. https://doi.org/10.1190/1.1443535

Saibi H, Nishijima J, Ehara S, Aboud E (2006) Integrated gradient interpretation techniques for 2D and 3D gravity data interpretation. Earth Planet Sp 58(7):815–821. https://doi.org/10.1186/BF03351986

Sarkowi M, Wibowo RC, Minardi S, Arifianto I (2021) Identification of Hydrocarbons Sub-Basin Based on Gravity Data Analysis in Lampung Area. J P F A 11(2):106–113. https://doi.org/10.26740/jpfa.v11n2.p106-113

Spector A, Grant FS (1970) Statistical Models for Interpreting Aeromagnetic Data. Geophysics 35(2):293–302. https://doi.org/10.1190/1.1440092

Sumintadireja P, Dahrin D, Grandis H (2018) A Note on the Use of the Second Vertical Derivative (SVD) of Gravity Data with Reference to Indonesian Cases. J Eng Technol Sci 50(1):127–139. https://doi.org/10.5614/j.eng.technol.sci.2018.50.1.9

Telford WM, Geldart LP, Sheriff RE (1990) Applied Geophysics, 2nd edn. Cambridge University Press